IEEE Open Journal on
Immersive Displays

Received 1 October 2023; revised 1 December 2023; accepted 4 December 2023. Date of publication 13 December 2023; date of current version 29 December 2023. The review of this article was arranged by Associate Editor Prof. Arokia Nathan.

Digital Object Identifier 10.1109/OJID.2023.3342769

High Picture Quality Quantum-Dot Light-Emitting Diode Display Technologies for Immersive Displays

JEONG-WAN JO [1], YOONWOO KIM [1], JIAJIE YANG [1], SANGHYO LEE [1,2], SUNG-MIN JUNG [1], LUIGI GIUSEPPE OCCHIPINTI [1] (Senior Member, IEEE), AND JONG MIN KIM [1]

(Review Paper)

[1]Electrical Engineering Division, Department of Engineering, University of Cambridge, CB3 0FA Cambridge, U.K.
[2]School of Materials and Engineering, Kumoh National Institute of Technology, Gumi 39177, South Korea

CORRESPONDING AUTHOR: SUNG-MIN JUNG (e-mail: sj569@cam.ac.uk).

This work was supported in part by the U.K. Engineering and Physical Sciences Research Council (EPSRC) "Smart Flexible Quantum Dot Lighting" under Project EP/P027628/1 and in part by the European Union under H2020 Grant 685758 '1D-NEON'.

ABSTRACT High-resolution microdisplays that offer superior picture quality are pivotal display components in immersive augmented reality (AR) and virtual reality (VR) systems. For AR and VR applications, the microdisplays must satisfy major requirements such as high resolution, exceptional brightness, and a broad color gamut to ensure clear and vivid picture quality. Quantum-dot light-emitting diodes (QD-LEDs) are emerging light sources due to their outstanding color purity and controllability. Rapid advancements in QD materials and device technologies suggest the potential industrialization of QD-LED displays in the near future. Moreover, recent innovation in the process technology of patterning QD layers enables the formation of ultrahigh-resolution QD-LED pixels for microdisplays, promising immersive and brighter visual experiences in AR and VR applications. In this study, we review the latest QD-LED technologies from QD material advancements and device architecture optimization to the pixelization process and integration of full-color display systems. Advancements in QD-LED display technology will enable the realization of high picture quality QD-LED microdisplays for extremely immersive AR and VR display systems.

INDEX TERMS Immersive displays, augmented reality, virtual reality, quantum-dot light-emitting diodes, micro displays, high resolution, pixelization technologies.

I. INTRODUCTION

Recently, owing to the rapid growth in demand for interaction with the real world to provide natural and immersive user experiences, there has been extensive research on immersive displays that effectively deliver object-oriented or sight-integrated information [1], [2], [3], [4]. Immersive displays project stereoscopic 3D images to the left and right eyes through augmented reality (AR) or virtual reality (VR) display optical systems, revolutionizing a wide range of fields including but not limited to healthcare, medicine, communications, entertainment, gaming, education, product design, and manufacturing [5], [6], [7], [8], [9], [10], [11], [12].

VR display systems project a virtual image by eye-piece lenses that magnify the images on the display, effectively blocking out the surrounding environment to create an immersive experience within a virtual world such as the Metaverse concept. On the other hand, AR display systems project virtual images into the real world by see-through optics equipped with appropriate optical combiners, enhancing the user's perception of the real world [13]. The general requirements for AR/VR display systems include a wide field of view (FOV) to fully cover the user's eyesight, a high-resolution and bright image for clear vision, a wide color gamut for natural color representation, minimal motion artifacts, and a lightweight and compact form factor suitable for wearable applications [14], [15]. While the picture quality is influenced by the projection optics, the display performance significantly impacts most of the requirements for immersive displays. The major

requirements for displays used in AR and VR systems include high resolution, high brightness, wide color gamut, high contrast ratio, and high-speed response to meet the demands for superior image quality.

Apple Inc. announced to launch the Vision Pro equipped with a 23 million pixel organic light-emitting diode (OLED) display in 2024 [16]. Sony Corp. launched the PlayStation VR2 equipped with OLED displays having 2000 × 2040 pixels [17]. Recently, Sony Semiconductor Solutions announced the upcoming release of a 1.3-inch OLED micro display with 3552 × 3840 pixels, offering a resolution of 4000 pixels per inch (PPI) for AR and VR systems [18]. There are several candidate pixel architectures for ultrahigh-resolution displays such as i) blue emissive pixel arrays with red and green quantum-dot color conversion (QDCC) layers, ii) white emissive OLED pixel arrays with red, green, and blue color filter (CF) layers, iii) red, green, and blue independent micro-LED or OLED pixel arrays, and iv) red, green, and blue independent electrically driven quantum-dot light-emitting diode (QD-LED) pixel arrays [19], [20], [21]. Among these technologies, due to the fabrication process issue, white OLEDs with a CF layer architecture are currently viable for the commercialization of ultrahigh-resolution displays for AR and VR applications. Nevertheless, to display extremely vivid images for a more immersive experience with AR and VR systems, achieving a high-picture quality display with enhanced color purity and brightness is essential.

Due to the size-dependent color controllability of quantum dots (QDs) and high color purity resulting from their sharp emission bandwidth, QD-LEDs offer an exceptionally wide color gamut compared to other types of display devices, such as liquid crystal displays (LCDs), OLEDs, and gallium-nitride light-emitting diodes (GaN-LEDs) [22], [23]. Furthermore, owing to their high photoluminescence quantum yield (PLQY) and external quantum efficiency (EQE), QD-LEDs exhibit extremely high brightness [24]. Additionally, owing to their self-emissive device structure, they offer a high contrast ratio, enabling the implementation of a high dynamic range. Naturally, because of the electron-involved dynamics in photon generation across the device, QD-LEDs show a fast response time that minimizes motion blur artifacts. Recently, advances in pixelization technologies have enabled the fine patterns of QDs for high-resolution displays [25], [26]. Therefore, the QD-LED device is the strongest candidate for next-generation AR/VR immersive display systems [20].

To date, RGB full-color active-matrix (AM) QD-LED display systems have been developed with limited resolution on a thin-film transistor (TFT) backplane [27]. However, to achieve a full-color ultrahigh-resolution AM QD-LED display with super-high brightness, significant advancements and optimizations are needed in various aspects, including materials, devices, processes, and display systems. In this article, we review the fundamental concepts of QD-LEDs and the current progress in the development of QD materials, optimized device architectures, innovative fabrication processes, and recent development of QD-LED displays for immersive

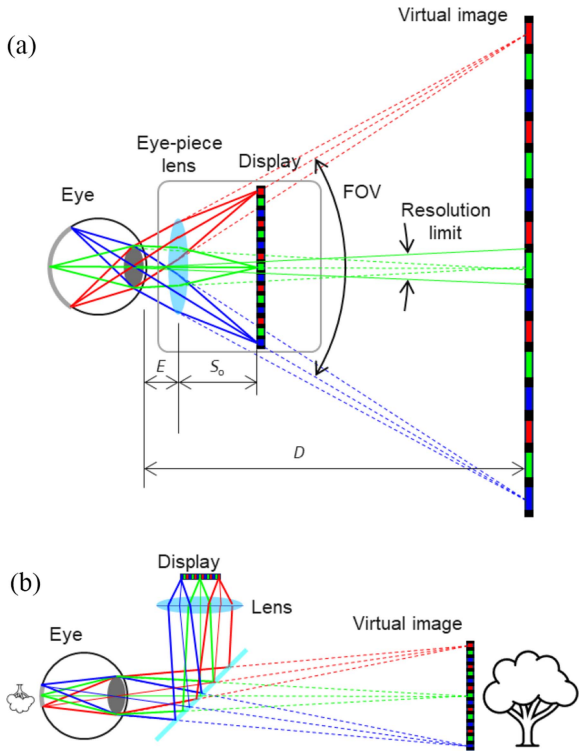

FIGURE 1. Optical configuration of immersive display systems. (a) VR and (b) AR display systems.

AR and VR display systems. First, the basic concept of an immersive AR/VR display system and the display requirements for the AR and VR systems will be discussed. Next, the properties of the QD nanoparticles including recent research highlights for high PLQY will be explored. Then, the operational principle of QD-LED devices and the state-of-the-art device engineering technologies for QD-LEDs will be discussed. The evolution of fabrication technologies, especially for precise QD patterning processes will be investigated. Finally, by summarizing the state-of-the-art development of full-color AM QD-LED display systems, the possibility of QD-LEDs for the application of immersive AR and VR systems will be discussed.

II. REQUIREMENTS OF DISPLAY FOR IMMERSIVE SYSTEMS

Fig. 1 shows the optical configuration of the typical AR and VR display systems in the form of near-eye displays (NEDs). In general, VR systems consist of a magnifying eye-piece lens in front of the eyes at a distance E and a small display engine located at a distance S_o from the magnifying lens with focal length f (Fig. 1(a)). The eye-piece lens magnifies the displayed image to form a virtual image at a distance D from the eye. Meanwhile, AR systems employ a similar magnifying optical configuration but with a transparent optical combiner to merge the displayed image with the real world (Fig. 1(b)). Various types of optical configurations are used for VR systems, including magnifying aspherical lenses,

Fresnel lenses, catadioptric pancake optics, and pin-light optics with microdisplays [3], [28]. The optical configurations for AR systems include birds-bath optics, freeform combiners, holographic optical element (HOE)-based combiners, and waveguide-type couplers with microdisplays [15], [29].

The general requirements for the AR/VR display systems include: i) a wide FOV to fully cover the eye-sight, ii) appropriate image distance to avoid vergence-accommodation conflict (VAC) that can lead to eye fatigue and discomfort, iii) high display resolution for crystal-clear vision, iv) high dynamic range with high contrast ratio and high brightness for vivid image, v) a wide color gamut to accurately represent natural colors, vi) minimized motion artifacts achieved through a high refresh rate and fast response time of the display, and vii) a lightweight and compact form factor suitable for eye-wear applications.

The size and resolution requirements of the display are determined by the magnification factor and FOV of the AR or VR optics. The perceptual limit of resolution for visual acuity of 20/20 is 1 arc minute, which is equivalent to 60 pixels per degree (PPD). Therefore, to exceed human perception, the resolution of the projected image should be greater than FOV $\times$ 60 PPD. Since the monocular horizontal FOV is 160°, and the vertical FOV is approximately 100° [21], [30], to fully cover the FOV while surpassing perceptual resolution, 9600 $\times$ 6000 pixels are needed in the horizontal and vertical directions. In terms of the display size, if we choose a vertical size of 1.5 inches as an example, 6000 pixels should be integrated within the size; hence, a resolution of 4000 PPI is needed. Assuming a 1:1 pixel aspect ratio, the horizontal display size should be 2.4 inches, and the pixel size should not exceed 6.35 μm $\times$ 6.35 μm.

Meanwhile, the luminance requirements for display in AR and VR applications can be determined by the ambient contrast ratio (ACR) defined in (1) [2].

$$ACR = \frac{L_{on} + L_{amb} \cdot T}{L_{off} + L_{amb} \cdot T} \tag{1}$$

Here, L_{on} and L_{off} represent the luminance in the on and off states of the display, L_{amb} denotes the luminance for the ambient brightness, and T signifies the transmittance of the AR or VR system. In the case of VR systems, to facilitate an immersive experience, the surrounding environment is completely blocked out; hence, T can be considered to be zero. Consequently, the ACR of VR systems closely matches the contrast ratio of the display. Therefore, the current display brightness level of 300 cd/m^2 is sufficient for use in VR systems. However, for AR systems, a much higher display brightness is needed for use in daylight conditions. For instance, an ambient brightness B of 10^4 lux for daylight corresponds to a luminance L_{amb} of 3183 cd/m^2 ($L_{amb} = B/\pi$ for Lambertian distribution). Assuming an ambient transmittance of 80%, a display brightness of 10185 cd/m^2 or 22918 cd/m^2 is needed to achieve a 5:1 or 10:1 ACR in an AR system.

Based on the above calculations, achieving extremely high-performance displays with ultrahigh pixel resolution and ultrahigh brightness is necessary for AR and VR applications to provide fully immersive experiences beyond human perception. In the following section, we will explore QD-LED display technologies, including QD nanomaterials, device architectures, fabrication processes, and QD-LED displays as potential candidates for achieving these requirements for immersive AR and VR display systems.

III. QD MATERIAL DESIGN AND SYNTHESIS

Fig. 2(a) shows the material structure of the QD nanoparticles. A QD is composed of i) a core nanocrystal, ii) a shell layer, and iii) a surface-binding ligand [23], [31], [32], [33], [34], [35]. The core nanocrystal generates light through a radiative recombination process of excitons confined in the core region. Commonly used core nanocrystal materials include cadmium selenide (CdSe), indium phosphide (InP) and zinc telluride selenide (ZnTeSe). The shell layer provides a quantum confinement effect with a high energy barrier height for the electrons and holes (Fig. 2(b)) [36], [37], [38]. Common materials used for the shell layer include cadmium sulfide (CdS), zinc sulfide (ZnS), and zinc selenide sulfide (ZnSeS) depending on the composition of the core materials. The surface-binding ligand passivates the shell layer of the QD nanoparticles from oxygen and moisture to prevent the degradation of particles. It also increases colloidal stability by inhibiting the aggregation of QDs in a selective solvent [39], [40]. Commonly used materials for surface-binding ligands include oleic acid and oleylamine. A snapshot of the QD nanoparticles captured by transmission electron microscopy (TEM) is shown in Fig. 2(c).

The wavelength of the emitted light Is determined by the optical bandgap, which is controlled by the size and material composition of the core nanocrystals (Fig. 2(d) and (e)). For typical red, green, and blue light emissions with peak wavelengths of 630 nm, 530 nm, and 450 nm, the diameters of CdSe QD cores are 7.0 nm, 4.6 nm, and 3.6 nm, respectively, while those of InP QD cores are 3.7 nm, 3.4 nm, and 3.2 nm (Fig. 2(f)), respectively. The size-dependent color controllability of QDs can be utilized in a wavelength-selective optical system, such as an HOE combiner, to create a new type of AR and VR platform. The photoluminescence of solution-state QDs is shown in Fig. 2(g) and (h) under both natural light and UV light. Red, green, cyan, and blue lights are emitted when they absorb UV light energy exceeding their respective optical bandgaps. Emission properties are characterized by the peak emission wavelength and the full width at half maximum (FWHM) of the emission spectrum. The material efficiency of QDs is quantified by the PLQY, which is measured by the ratio between the absorbed light energy S_a and the emitted light energy S_e (Fig. 2(i)).

The lifetime of the QD-LED device is directly influenced by the stability of the QDs, which is degraded by the reaction with oxygen, water, and other factors such as heat and UV light [17]. One way to enhance device lifetime is to optimize the material and the structure of the shell and ligand [39], [41]. Depending on the thickness of the shell and the length of the

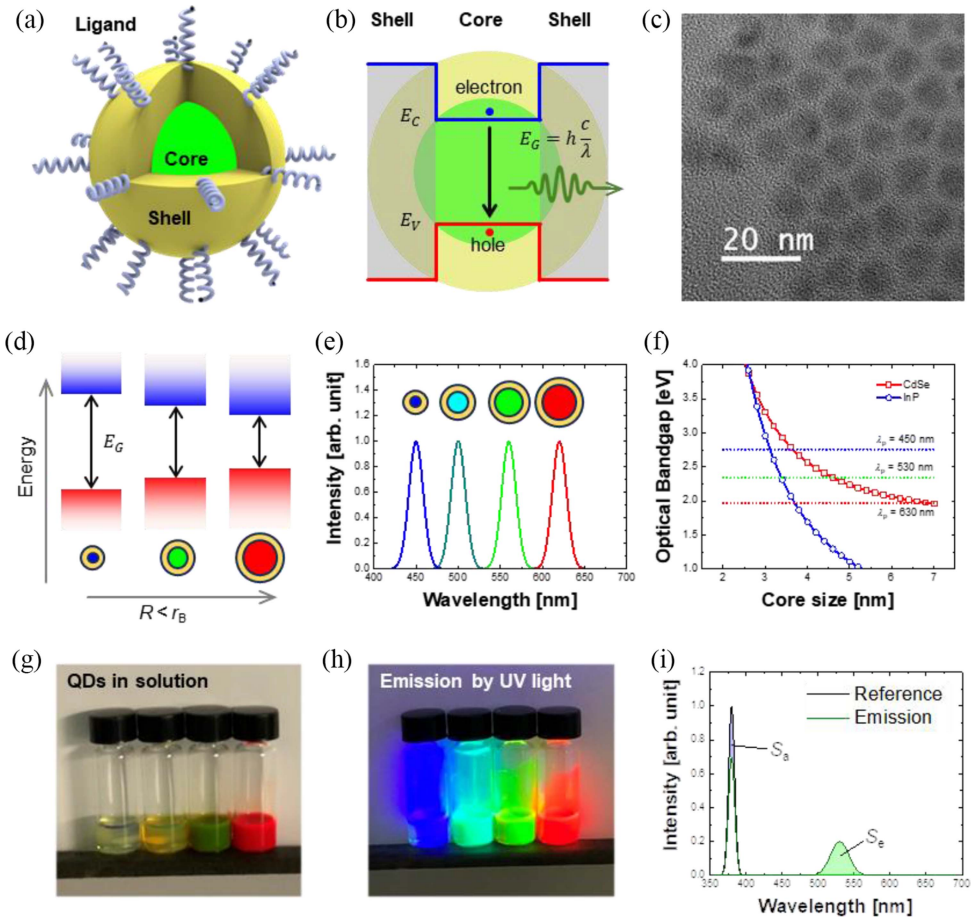

FIGURE 2. QD nanoparticles and their optical properties. (a) Structure and (b) energy-level configuration of a single QD nanoparticle. (c) TEM image of QD nanoparticles. Size dependencies of (d) energy band levels and optical bandgap and (e) their emission spectra. f) Optical bandgap with respect to the core size. (g) QDs in solution under natural light and (h) photoluminescence of QDs under UV stimulus. (i) PLQY measurement of QDs.

surface-binding ligand, a trade-off relationship exists between colloidal stability in the solution and charge transport in the QD-LED device [42], [43]. Therefore, careful attention to the shell layer and surface-binding ligand is needed to optimize the material composition and architecture of the QD nanoparticles.

Considerable advancements have been achieved in the development of QDs to attain high PLQY, uniform size distribution and material stability. Cd-based QDs have served as a primary platform material and have been extensively utilized to optimize nanoparticle architecture by incorporating engineered shell and surface-binding ligands. By fine-tuning the materials and thicknesses of the shell layers, lattice mismatches between the core and shell were minimized, resulting in enhanced PLQY values. To secure material stability, a concept involving electrochemically stable surface-binding ligand exchange has been introduced, reducing the degradation of QD nanoparticles from surface oxidation and ionization. Recent achievements with Cd-based QDs include PLQY values exceeding 97% for red [44], 90% for green [45], and 87% for blue [46]. Commercially available QD nanoparticles exhibit more than 90% PLQY based on Cd-based QD materials with FWHM less than 30 nm [47].

Although most of the literature reporting the highest performance relies on Cd-based QDs [45], [48], [49], [50], there is an urgent demand for Cd-free QDs due to environmental concerns. High-performance red, green, and blue InP-based QDs have been reported with impressive PLQY values of 98%, 95% and 80%, respectively, through a process involving hydrogen fluoride (HF)-based surface etching, the introduction of Zn-oxo complex, and gallium (Ga) alloying into the InP core [24], [51], [52]. In addition to InP-based QD materials, ZnTeSe has also been employed as the emissive core material for blue QDs. Utilizing a ZnS/ZnTeSe/ZnS (core/mid-layer/shell) structured QD, a remarkable PLQY of 85% was achieved [53]. More recently, blue QDs based on ZnTeSe with almost 100% PLQY have been developed by incorporating HF acid and zinc chloride as additives during the QD synthesis process [54].

IV. QD-LED DEVICE ARCHITECTURE

To fully utilize the superior electro-optical properties of QD nanoparticles, extensive research has been dedicated to the development of QD-LED device architectures [55], [56], [57], [58]. Fig. 3 outlines the architectures and operational principles of the QD-LED device. QD-LEDs consist of a stack of

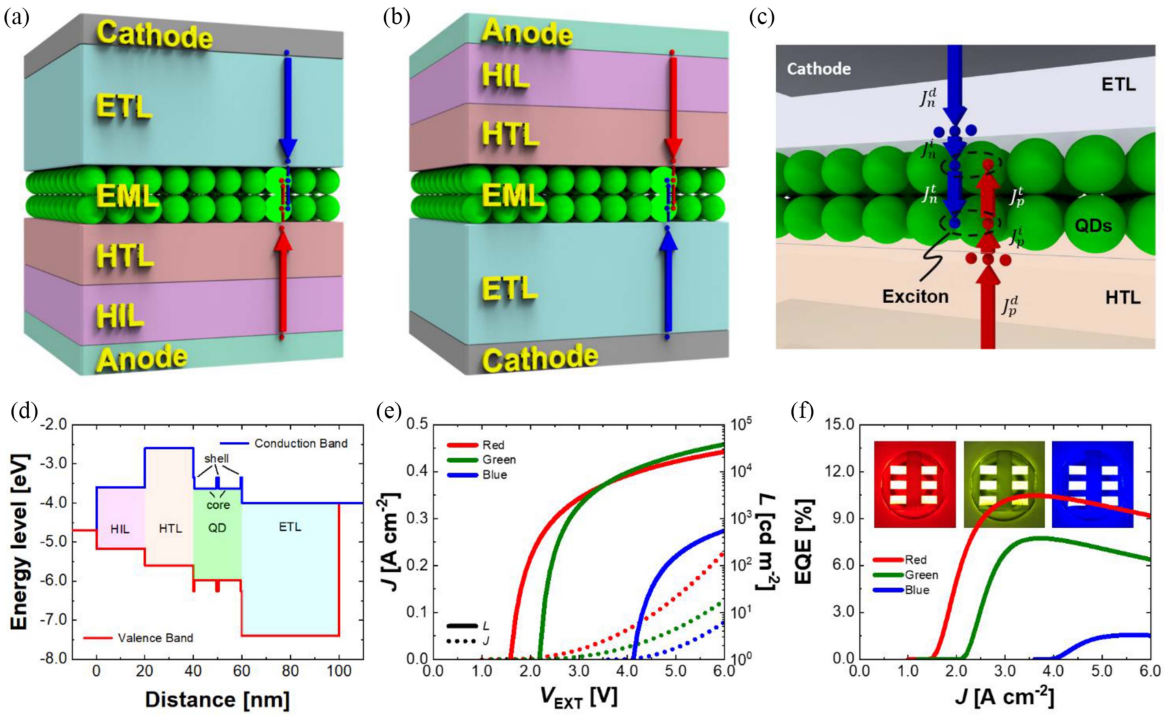

FIGURE 3. Device architecture and the charge transport mechanism of QD-LEDs. (a) Bottom emission structure. (b) Top emission structure. (c) Charge transport mechanism in the vicinity of the QD layer. (d) Example of a flat-band energy-level diagram across the device. (e) Examples of current (*J*) – voltage (*V*) – luminance (*L*) curves for red, green, and blue QD-LEDs. (f) Examples of EQE curves for red, green, and blue QD-LEDs with inset snapshots of red, green, and blue devices.

multiple semiconductor layers, which include a hole injection layer (HIL), a hole transport layer (HTL), an emissive layer (EML), and an electron transport layer (ETL). This stack is then sandwiched between the anode and cathode electrodes, as depicted in Fig. 3(a) and (b). There are two primary types of QD-LED device architectures: the conventional structure (Fig. 3(a)) and the inverted structure (Fig. 3(b)). The choice of device architecture depends on the specific application and operation condition of the QD-LEDs. The conventional structure is widely used for bottom emission QD-LEDs, where light is emitted through the transparent bottom indium tin oxide (ITO)/glass substrate [48], [59], [60]. However, for AR/VR applications, top emission device architectures that are formed on top of the transistor array are suitable due to the lack of the aperture ratio caused by the compact integrity of transistor circuits in each pixel. This conventional structure is also reconfigured for top-emission QD-LEDs by utilizing an Al/ITO double electrode for the anode and a silver-magnesium (AgMg) thin electrode for the transparent cathode. On the other hand, inverted QD-LEDs are preferred for AR/VR applications as they are top emission structures when an n-type channel oxide TFT is used for the AM addressing, owing to their bottom cathode structure [60], [61], [62], [63].

The commonly used materials for the anode and cathode electrodes are ITO and aluminum (Al), respectively. Poly (34-ethylene dioxythiophene)-poly(styrene sulfonate) (PEDOT:PSS) is a common material for the HIL. Commonly used materials for the HTL include poly[(99-dioctylfluorenyl-27-diyl)-co-(44′-(N-(4-sec-butyl phenyl)diphenylamine)] (TFB), poly(4-butyl-phenyldiphenyl-amine) (Poly-TPD) and/or poly-N-vinyl carbazole (PVK). Zinc oxide (ZnO) nanoparticles are widely used as ETL materials [64]. The EML, which is composed of QD nanoparticles, plays a crucial role in light emission.

The flat-band energy diagram across the device, from the anode to cathode electrodes, is plotted in Fig. 3(c) illustrating the valence and conduction energy band offsets, ΔE_V and ΔE_C, at the HTL/EML and EML/ETL interfaces. Under a positive external bias voltage, holes and electrons are transported from external voltage sources, being directed into the HTL/EML and EML/ETL interfaces and accumulating at the surfaces of the HTL and ETL adjacent to the EML layer [22], respectively. Subsequently, the accumulated holes and electrons are injected into the EML, surmounting the band offsets through the electric-field-dependent charge-capturing process (Fig. 3(d)) [22], [65]. Following the injection process, holes and electrons within the QD nanoparticles are transferred to the neighboring QD nanoparticles via carrier exchange process, facilitated by quantum tunneling effects [66], [67], [68]. Due to the high energy barrier between QDs and the ETL or HTL, acting as carrier-blocking layers, respective holes and electrons are blocked to the opposite side. Consequently, holes and electrons accumulate in the QD layer, forming excitons for radiative recombination to generate light in QD core nanocrystals.

The threshold voltage of the QD-LED devices is determined by device parameters such as the band offsets on the valence band (ΔE_V) and conduction band (ΔE_V), the number of QD layers M in the EML, and the work function difference V_{bi} between the cathode and anode electrodes with proton charge q, as shown in (2) [22].

$$V_{th} = \frac{2M}{q} \max\left(\Delta E_C, \Delta E_V\right) + V_{bi} \tag{2}$$

The maximum EQE of the QD-LED device $\eta_{EQE,MAX}$ is determined by the recombination process, which is influenced by the core crystalline properties of QD nanoparticles, such as the Langevin radiative recombination strength γ, Shockley-Read-Hall nonradiative recombination lifetime τ, and the Auger nonradiative recombination probability C with the PLQY of the QD layer η_{PHT}, as shown in (3) [26].

$$\eta_{EXT,MAX} = \eta_{PHT} \frac{\gamma/\sqrt{C/\tau}}{\gamma/\sqrt{C/\tau} + 2} \tag{3}$$

The device lifetime is closely associated with the configuration of layers within the QD-LED device. The main factor contributing to performance degradation, from the device perspective, is the unbalanced injection of holes and electrons into the QDs, resulting in the charging of QDs and nonradiative Auger recombination due to excessive charges within the QD layer [48]. Charge injection is influenced by various physical parameters, including carrier mobility, conduction and valence energy levels, carrier concentration, and the interface and surface morphology of the HIL, HTL, ETL and EML. Therefore, by engineering each of the transport layers, it becomes possible to achieve charge balance, maximize electro-optical performance and extend the device lifetime. Many studies related to the engineering of ETL/HTL, employing various materials and fabrication methods, have been reported. Recent studies have even achieved the theoretical maximum EQE for QD-LED devices [24], [45], [54], while enhancing the device lifetime remains one of the primary challenges for the commercialization of QD-LEDs. In the following, the most relevant reports on device optimization aiming for higher EQE and a longer lifetime are introduced.

Shen et al. achieved high-performance Cd-based QD-LEDs with a bottom emission device architecture showing EQEs of 21.6%, 22.9% and 8.1% for red, green and blue devices, respectively. These devices exhibited impressive lifetimes, with T50@100 cd/m^2 values of 1600000 hours, 1760000 hours and 7000 hours for red, green, and blue, respectively. These exceptional results were obtained by utilizing high PLQY QDs and QD layers with highly qualified surface morphology [45]. Alexandrov et al. optimized the ETL by employing Al-doped ZnO with high electron conductivity, well-aligned energy band levels, and smooth surface morphology [69]. Al-doped ZnO has become a popular material for ETLs. Dai et al. demonstrated efficient Cd-based red QD-LEDs with a threshold voltage of 1.7 V, a remarkable EQE of 20.5%, and a long lifetime (T50@100 cd/m^2) exceeding 100000 hours. These performances are achieved by introducing a hole-blocking layer with a very thin polymethyl methacrylate (PMMA) layer to establish charge-balanced conditions within the device [70].

Based on the inverted device architecture (top emission), QD-LED devices with enhanced performances have been achieved by incorporating an interfacial modification layer (IML) between ZnO (ETL) and QDs [49], [71]. The IML serves to block excessive charges and passivate defect states in ZnO. The presence of the IML suppresses exciton quenching and improves charge balance conditions. Lee et al. demonstrated another inverted structure, which exhibited reduced leakage current along with enhanced device performance [49], [71]. To break through the EQE performance, a hybrid device architecture in a tandem structure has also been reported [30], [43], [44], [45], [46], [47]. Zhang et al. demonstrated high-performance tandem structure Cd-based QD-LEDs, achieving high EQEs over 23.1%, 27.6%, and 21.4% for red, green and blue devices, respectively. This was accomplished by serially stacking two or more QD-LED units with an interconnecting layer (ICL) [72]. Won et al. presented InP-based red QD-LED devices with 21.4% EQE, a brightness of 100000 cd/m^2, and an extremely long lifetime of 1000000 hours. They achieved these results by engineering the shell thickness and exchanging the ligands of QD nanoparticles to improve charge injection [24]. Kim et al. also demonstrated ZnTeSe-based blue QD-LED devices having an EQE of 20.2%, a brightness of 88900 cd/m^2, and a long operating lifetime of 15850 hours at T50@100 cd/m^2. This was achieved by employing double QD emitting layers with a gradient chloride content to facilitate hole transport [54].

V. QD-LED PIXELIZATION PROCESS

The most common process for fabricating a QD-LED device is a solution-based spin-coating process [73]. The spin-coating method provides uniform thin films with nanoscale thickness. The thickness of the QD layer is determined by the QD concentration in the solution and the spin speed during the coating process. It is important to note that the electro-optical performance and device stability of the QD-LED are influenced by both the film thickness and the quality of the QD layer. Given that the diameter of QD nanoparticles is below 10 nm, it is essential to fabricate a closely packed QD layer as thin as possible without voids to maximize the light efficiency and device lifetime [74]. Therefore, when adapting the solution process for larger-scale display applications, maintaining a uniform thickness and ensuring good surface morphology become crucial for achieving high-quality QD films. However, due to the inherent limitations of the spin-coating process, achieving spatial separation of red, green, and blue QD subpixels for full-color display applications with electrically driven QD-LEDs is unfeasible with spin-coating alone. Several techniques are employed to form QD patterns, including inkjet printing, photolithography, and transfer printing.

Inkjet printing, a non-contact, mask-free technique, is extensively utilized for pixel patterning by propelling QD ink droplets onto specific locations. It is commonly employed

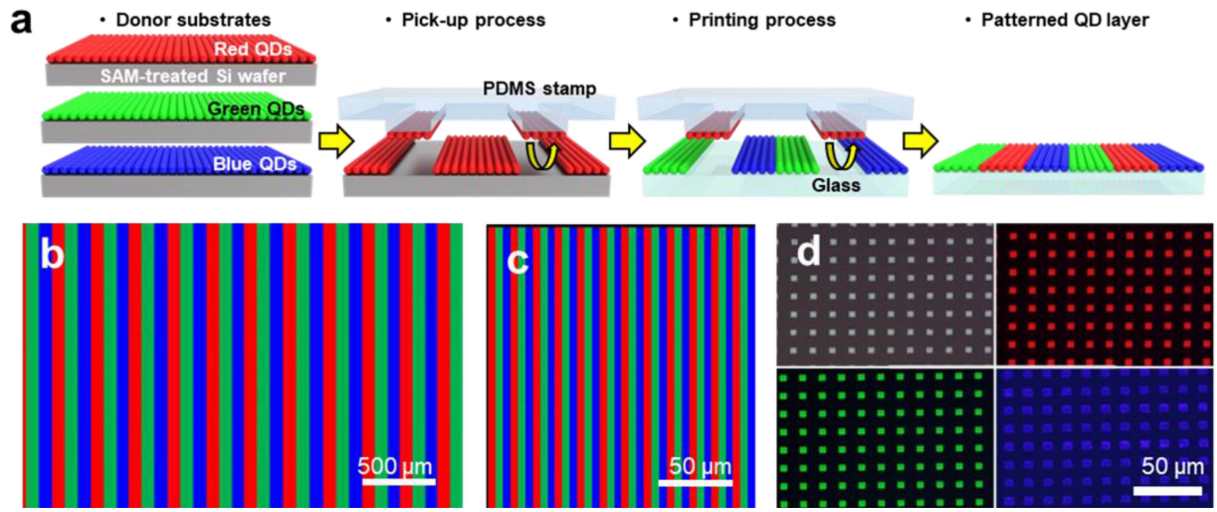

FIGURE 4. QD Pixelization process and AM EL QD-LED-based displays. (a) Transfer printing process for patterning the QD layer. (b) Stripe QD patterns of (b) 85 μm and (c) 50 μm widths for red, green, and blue QDs. (d) 5 μm square QD patterns for PDMS stamps and red, green, and blue QDs.

not only for QD-LED displays but also for QDCC layers. Moreover, inkjet printing equipment has advanced with precise control and monitoring solutions, attracting considerable interest from the industry. Despite its large-area process feasibility for QD patterning, the performance of inkjet-printed QLEDs requires improvement to catch up with the state-of-the-art results of spin-coated devices. Additionally, inkjet printing faces challenges when trying to create QD pixels smaller than a few micrometers due to difficulties in controlling the size of ink droplets, ink formulation-dependent coffee ring effect, and nozzle clogging [75], [76], [77].

The photolithography technique, a well-established nano-/micro-scale patterning process in the semiconductor industry, photocopies patterns from photomasks to photosensitive chemicals using UV light. In applying this technique to QD patterning, QDs are typically mixed with a negative photoresist solution and exposed to UV light through a photomask [78]. The unexposed parts are selectively removed by a developer and repeated to generate various QD patterns on the same substrate. An alternative method involves separately coating photoresist and QDs, combined with a lift-off process to minimize residual organic content [79]. More recent research has explored the use of ligand molecules on QD surfaces as photosensitive chemicals for photoresist-free methods [80]. However, challenges remain in the photolithography process, such as potential damage to QDs and charge transport layers from organic solvents and high UV energy exposure, the risk of cross-contamination of red, green, and blue QDs during development [81], and interferences with charge transport due to the presence of photoresist/organic residues, leading to the degradation of device performance [82], [83], [84], [85], [86], [81].

The transfer printing technique has innovated the pixelization of the QD layer, allowing for pixel sizes down to a few micrometers for display applications and preventing contamination of the pixels during the process [25], [26], [74], [87], [88], [89]. Fig. 4(a) depicts a schematic illustration of the typical fabrication process flow for pixels using the transfer printing technique. QDs of individual colors are picked up by using a patterned polydimethylsiloxane (PDMS) stamp from a self-assembled monolayer (SAM)-treated donor substrate. These QDs are then transferred onto a preprocessed charge transport layer using transfer printing equipment. The micropatterns of PDMS stamps are replicated from a master mold created by a photoresist on a silicon wafer through a photolithography process. The shape of the individual QD layer is duplicated by the shape of the micropatterns on the PDMS stamps. By repeating the pick-up and transfer printing processes for red, green, and blue QDs with precise alignment, pixelated QD layers are formed at spatially separated locations. Fig. 4(b)–(d) display microscopy images of various red, green, and blue QD pixel patterns, ranging from 50 μm and 5 μm stripes to 5 μm dot features, all fabricated through the transfer printing process in our group.

The concept of transfer printing using a PDMS stamp was introduced as an alternative to the solution-based wet spin-coating process [74], [90]. Profiled PDMS stamps are used to create red, green, and blue monolayer QD patterns for the application of white lighting [91]. Additionally, a layer-by-layer transfer printing technology of heterogeneous QD stacks has been reported, allowing for reliable transfer printing of QD monolayers to create a new device architecture for white LED applications [92]. Kim et al. demonstrated the first 4-inch AM driving electroluminescence (EL) full-color QD display system using a transfer printing technique to create an emissive pixel area of 46 μm $\times$ 96 μm [27]. The independent donor substrates with SAM treatment enable the transfer printing of uniform monolayers of red, green, and blue QDs onto the target substrate. The maximum EL peaks for the printed red, green, and blue QLEDs are observed at wavelengths of 615 nm, 530 nm, and 480 nm, respectively. The corresponding maximum brightness values

are 16380 cd/m^2 for red, 6425 cd/m^2 for green, and 423 cd/m^2 for blue. The maximum brightness and luminous efficiency of the transfer-printed QD-LED were approximately 25-52% higher in all cases, with a remarkable 71% maximum power efficiency improvement observed in the transfer-printed red QLED compared to the spin-coated QLED. The reduction in leakage current and improvement in the luminous efficiency of the QLED can be attributed to the solvent-free dry transfer printing process. This method enhances the charge transport properties by facilitating the close packing of the QD film through the pressure applied by the PDMS stamp [88] without damaging the HTL layer.

Transfer printing techniques have advanced further to precisely fabricate QD pixel patterns for extremely high pixel resolution. A smaller pixel size was fabricated using an intaglio transfer printing technique for AR and VR applications. Choi et al. demonstrated the integration of 5 μm-sized red, green, and blue subpixels, showcasing the potential for a high resolution of up to 2460 PPI [93], [94]. Instead of patterned PDMS, they introduced an intaglio trench to eliminate unwanted areas on the QD layer of a flat PDMS. Recently, Nam et al. created integrated red, green, and blue pixel patterns with subpixel sizes of 50 μm, 12 μm, 4 μm, 3 μm, and 0.5 μm for VR application using thermodynamic-driven immersion transfer printing [95]. Meng et al. achieved monochromatic pixels of 0.5 μm in size with a 0.5 μm gap, resulting in a 25400 PPI monochromatic display through a transfer printing process combined with Langmuir-Blodgett film technology [96].

Although there have been significant advances in transfer printing techniques in terms of high-resolution patternability, several challenges remain for future transfer printing techniques: i) compatibility with nontoxic cadmium-free QD materials, ii) scalability toward nanoscale with high throughput for large-scale manufacturing, iii) performance comparable to spin-coated devices after patterning, and iv) transfer printing suitable for intricate structures such as a bank-structured pixel-defining layer. Therefore, by utilizing innovative transfer printing technology to form micron-sized QD pixels on a single crystalline-based AM array, it is anticipated that ultrahigh pixel density can be achieved, paving the way for realization of extremely immersive AR and VR systems.

VI. QD-LED DISPLAY SYSTEMS

To implement a full-color AM EL QD-LED display, red, green, and blue QD-LEDs integrated with transistors capable of controlling individual pixels should be precisely formed at each subpixel. Depending on the display applications, transistors for AM driving are divided into two categories: i) TFTs with a-Si, low-temperature polysilicon (LTPS), or indium gallium zinc oxide (IGZO) channel materials, and ii) metal oxide silicon (MOS) transistors with crystalline silicon channels. TFTs are mainly utilized by large area displays such as mobile, notebook, monitor, or TV applications, while MOS transistors are preferred to ultrahigh resolution displays for AR/VR applications owing to their small channel length feature for micrometer-sized pixels.

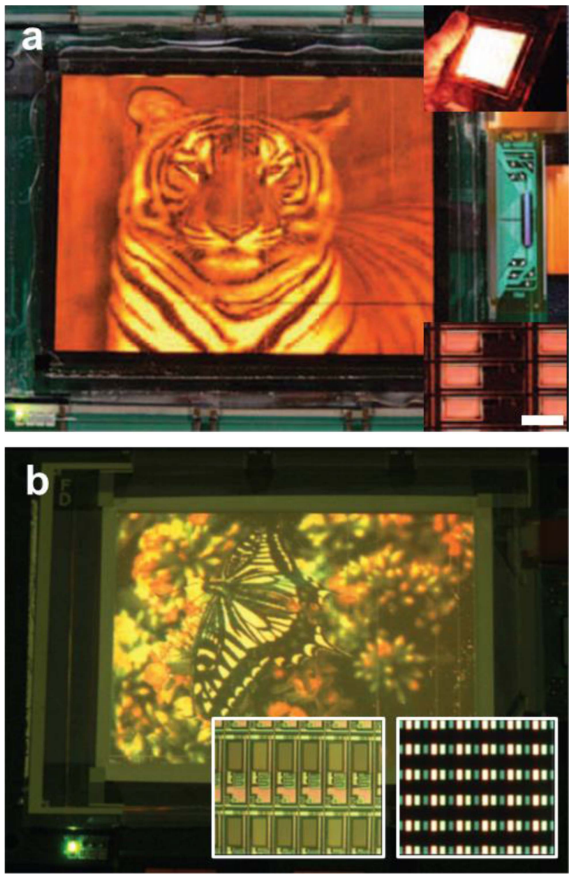

FIGURE 5. Development of QD-LED-based AM display systems. (a) 4-inches monochromatic red QD-LED AM display using an a-Si TFT backplane with a 320 × 240 pixel array. Reproduced with permission from Ref. [97]. Copyright 2009, Springer Nature. (b) a full-color QD-LED display using HIZO TFT-based AM with sequential transfer printing of RGB QDs. Reproduced with permission from Ref. [27]. Copyright 2011, Springer Nature.

Cho et al. presented the world's first 4-inch monochromatic red QD-LED AM display using an a-Si TFT backplane with a 320 × 240 pixel array (Fig. 5(a)). The device exhibited uniform brightness with less than 5% variation over a 4-inch display area [97]. Kim et al. developed a full-color QD-LED display using hafnium-indium-zinc oxide (HIZO) TFT-based AM with sequential transfer printing of RGB QDs [27]. BOE Technology Group Co., Ltd. demonstrated full-color AM QD-LED displays with a 5-inch LTPS TFT and 14-inch IGZO TFT backplanes using an all-inkjet printing process (IJP) [98], [99]. Sharp Corp. presented a full-color AM QD-LED display with 540 × 960 pixels for 176 PPI resolution using photolithography and a top emission EL device architecture based on IGZO TFTs [78], [100], [101]. Recently, Samsung Display Co., Ltd. demonstrated a 217 PPI 6.95-inch full-color AM Cd-free QD-LED display with an LTPS TFT array using an inkjet process and a top emission EL device architecture [102].

To date, QD-LED-based ultrahigh-resolution full-color AM displays for AR and VR applications have not yet been reported. Given the superior color properties of QDs, AM driving full-color EL QD-LED displays will deliver outstanding image quality with an extensive color gamut. Furthermore, the remarkable size-dependent color controllability of QDs can also be utilized to enhance the form factor of AR and VR systems through innovative optical designs. In summary, it is expected that QD-LED-based full-color AM displays, coupled with ultrafine transistor arrays, will pave the way for highly immersive experiences in next-generation AR and VR display applications.

VII. CONCLUSION

In this study, recent advancements in QD-LED display technologies are summarized, focusing on enhancing ultrahigh resolution and superior picture quality in immersive AR/VR display applications. We review the performance requirements of displays for AR/VR applications and explore the latest technologies in QD material synthesis, device optimization, and fabrication processes. Noteworthy progress has been made in the performances of QD materials through strategic engineering of the shell layer and surface-binding ligands, achieving a PLQY of over 95% and an FWHM of less than 30 nm. The development of environmentally free QD core materials has further enabled the commercialization of QD-LEDs. Moreover, through meticulous design and optimization, the EQE of red, green, and blue QD-LED devices has exceeded 20%, with a lifetime surpassing 100000 hours. Continued advancements, particularly in Cd-free QD-LED devices, are anticipated. Advancements in transfer printing technologies have enabled ultrafine patterning of red, green, and blue QD-LED pixels in micron-sized layouts. Recent progress in the development of QD-LED-based full-color AM displays showcases their potential for integration with ultrafine transistor arrays. Combinatorial innovations in QD material synthesis, device optimization, pixel fabrication processes, and integration with ultrafine transistor arrays enable ultrahigh-resolution full-color QD-LED displays with a wider color gamut, thereby facilitating high-quality AR and VR display systems for immersive user experiences.

REFERENCES

[1] O. Cakmakci and J. Rolland, "Head-worn displays: A review," *J. Display Technol.*, vol. 2, no. 3, pp. 199–216, Sep. 2006, doi: 10.1109/JDT.2006.879846.

[2] J. Xiong, E.-L. Hsiang, Z. He, T. Zhan, and S.-T. Wu, "Augmented reality and virtual reality displays: Emerging technologies and future perspectives," *Light Sci. Appl.*, vol. 10, no. 1, Oct. 2021, Art. no. 216, doi: 10.1038/s41377-021-00658-8.

[3] K. Yin, Z. He, J. Xiong, J. Zou, K. Li, and S.-T. Wu, "Virtual reality and augmented reality displays: Advances and future perspectives," *J. Phys. Photon.*, vol. 3, no. 2, Apr. 2021, Art. no. 022010, doi: 10.1088/2515-7647/abf02e.

[4] H.-J. Guo, J. Z. Bakdash, L. R. Marusich, and B. Prabhakaran, "Augmented reality and mixed reality measurement under different environments: A survey on head-mounted devices," *IEEE Trans. Instrum. Meas.*, vol. 71, 2022, Art. no. 5025115, doi: 10.1109/TIM.2022.3218303.

[5] E. Waisberg et al., "The future of ophthalmology and vision science with the apple vision pro," *Eye*, pp. 1–2, Aug. 2023, doi: 10.1038/s41433-023-02688-5.

[6] R. Kramme et al., *Springer Handbook of Medical Technology*. Berlin, Germany: Springer, 2011.

[7] L. Bryant, M. Brunner, and B. Hemsley, "A review of virtual reality technologies in the field of communication disability: Implications for practice and research," *Disabil. Rehabil.: Assistive Technol.*, vol. 15, no. 4, pp. 365–372, May 2020, doi: 10.1080/17483107.2018.1549276.

[8] P. Cipresso, I. A. C. Giglioli, M. A. Raya, and G. Riva, "The past, present, and future of virtual and augmented reality research: A network and cluster analysis of the literature," *Front. Psychol.*, vol. 9, Nov. 2018, Art. no. 2086, doi: 10.3389/fpsyg.2018.02086.

[9] N. Faric et al., "What players of virtual reality exercise games want: Thematic analysis of web-based reviews," *J. Med. Internet Res.*, vol. 21, no. 9, Sep. 2019, Art. no. e13833, doi: 10.2196/13833.

[10] T. N. Fitria, "Augmented reality (AR) and virtual reality (VR) technology in education: Media of teaching and learning: A review," *Int. J. Comput. Inf. Syst.*, vol. 4, no. 1, pp. 14–25, Feb. 2023, doi: 10.29040/ijcis.v4i1.102.

[11] D. Şahin and A. Togay, "Augmented reality applications in product design process," *Glob. J. Humanities Social Sci.*, vol. 3, pp. 115–125, 2016, doi: 10.18844/gjhss.v0i0.288.

[12] A. Y. C. Nee and S. K. Ong, "Virtual and augmented reality applications in manufacturing," *Int. Federation Autom. Control Proc. Volumes*, vol. 46, no. 9, pp. 15–26, 2013, doi: 10.3182/20130619-3-RU-3018.00637.

[13] D. Cheng et al., "Design and manufacture AR head-mounted displays: A review and outlook," *Light, Adv. Manuf.*, vol. 2, no. 3, pp. 350–369, 2021, doi: 10.37188/lam.2021.024.

[14] C. Chang, K. Bang, G. Wetzstein, B. Lee, and L. Gao, "Toward the next-generation VR/AR optics: A review of holographic near-eye displays from a human-centric perspective," *Optica*, vol. 7, no. 11, pp. 1563–1578, Nov. 2020, doi: 10.1364/OPTICA.406004.

[15] X. Xia, F. Y. Guan, Y. Cai, and N. M. Thalmann, "Challenges and advancements for AR optical see-through near-eye displays: A review," *Front. Virtual Reality*, vol. 3, Mar. 2022, Art. no. 838237, doi: 10.3389/frvir.2022.838237.

[16] "Introducing apple vision pro: Apple's first spatial computer," Jun. 2023. [Online]. Available: https://www.apple.com/uk/newsroom/2023/06/introducing-apple-vision-pro/

[17] "PlayStation VR2 tech specs," 2023. [Online]. Available: https://www.playstation.com/en-gb/ps-vr2/ps-vr2-tech-specs/

[18] "Sony semiconductor solutions to release large-size, high-definition 1.3-type 4K OLED microdisplay that reproduces realistic spaces enhancing the experiential value of VR and AR head-mounted displays," Aug. 2023. [Online]. Available: https://www.sony-semicon.com/en/news/2023/2023082401.html

[19] K. Yin et al., "Advanced liquid crystal devices for augmented reality and virtual reality displays: Principles and applications," *Light Sci. Appl.*, vol. 11, no. 1, May 2022, Art. no. 161, doi: 10.1038/s41377-022-00851-3.

[20] H. J. Jang, J. Y. Lee, G. W. Baek, J. Kwak, and J.-H. Park, "Progress in the development of the display performance of AR, VR, QLED and OLED devices in recent years," *J. Inf. Display*, vol. 23, no. 1, pp. 1–17, Jan. 2022, doi: 10.1080/15980316.2022.2035835.

[21] J. Ha et al., "Advanced VR and AR displays: Improving the user experience," *Inf. Display*, vol. 39, no. 2, pp. 15–19, Mar. 2023, doi: 10.1002/msid.1378.

[22] S.-M. Jung et al., "Modelling charge transport and electro-optical characteristics of quantum dot light-emitting diodes," *NPJ Comput. Mater.*, vol. 7, no. 1, Jul. 2021, Art. no. 122, doi: 10.1038/s41524-021-00591-9.

[23] S. Y. Bang et al., "Technology progress on quantum dot light-emitting diodes for next-generation displays," *Nanoscale Horiz.*, vol. 6, no. 2, pp. 68–77, 2021, doi: 10.1039/D0NH00556H.

[24] Y.-H. Won et al., "Highly efficient and stable InP/ZnSe/ZnS quantum dot light-emitting diodes," *Nature*, vol. 575, no. 7784, pp. 634–638, Nov. 2019, doi: 10.1038/s41586-019-1771-5.

[25] D.-W. Shin et al., "Color controllable smart white lighting based on various device architectures of electrically driven quantum-dot light-emitting diodes," *J. Mater. Chem. C*, vol. 10, no. 29, pp. 10728–10741, 2022, doi: 10.1039/D2TC01060G.

[26] C. Samarakoon et al., "Optoelectronic system and device integration for quantum-dot light-emitting diode white lighting with computational design framework," *Nature Commun.*, vol. 13, no. 1, Aug. 2022, Art. no. 4189, doi: 10.1038/s41467-022-31853-9.

[27] T.-H. Kim et al., "Full-color quantum dot displays fabricated by transfer printing," *Nature Photon.*, vol. 5, no. 3, pp. 176–182, Mar. 2011, doi: 10.1038/nphoton.2011.12.

[28] K. Bang, Y. Jo, M. Chae, and B. Lee, "Lenslet VR: Thin, flat and wide-FOV virtual reality display using Fresnel lens and lenslet array," *IEEE Trans. Vis. Comput. Graph.*, vol. 27, no. 5, pp. 2545–2554, May 2021, doi: 10.1109/TVCG.2021.3067758.

[29] Y.-H. Lee, T. Zhan, and S.-T. Wu, "Prospects and challenges in augmented reality displays," *Virtual Reality Intell. Hardware*, vol. 1, no. 1, pp. 10–20, Feb. 2019, doi: 10.3724/SP.J.2096-5796.2018.0009.

[30] T. Zhan, K. Yin, J. Xiong, Z. He, and S.-T. Wu, "Augmented reality and virtual reality displays: Perspectives and challenges," *iScience*, vol. 23, no. 8, Aug. 2020, Art. no. 101397, doi: 10.1016/j.isci.2020.101397.

[31] W. Guo, J. J. Li, Y. A. Wang, and X. Peng, "Luminescent CdSe/CdS core/shell nanocrystals in dendron boxes: Superior chemical, photochemical and thermal stability," *J. Amer. Chem. Soc.*, vol. 125, no. 13, pp. 3901–3909, Apr. 2003, doi: 10.1021/ja028469c.

[32] J. Zhou, M. Zhu, R. Meng, H. Qin, and X. Peng, "Ideal CdSe/CdS Core/Shell nanocrystals enabled by entropic ligands and their core size-, shell thickness-, and ligand-dependent photoluminescence properties," *J. Amer. Chem. Soc.*, vol. 139, no. 46, pp. 16556–16567, Nov. 2017, doi: 10.1021/jacs.7b07434.

[33] Y. Suh et al., "Engineering core size of InP quantum dot with incipient ZnS for blue emission," *Adv. Opt. Mater.*, vol. 10, no. 7, Apr. 2022, Art. no. 2102372, doi: 10.1002/adom.202102372.

[34] X.-B. Fan et al., "InP/ZnS quantum dot photoluminescence modulation *via in situ* H_2S interface engineering," *Nanoscale Horiz.*, vol. 8, no. 4, pp. 522–529, 2023, doi: 10.1039/D2NH00436D.

[35] A. R. C. Osypiw et al., "Solution-processed colloidal quantum dots for light emission," *Mater. Adv.*, vol. 3, no. 17, pp. 6773–6790, 2022, doi: 10.1039/D2MA00375A.

[36] A. I. Ekimov and A. A. Onushchenko, "Quantum size effect in three-dimensional microscopic semiconductor crystals," *J. Exp. Theor. Phys.*, vol. 34, 1981, Art. no. 345.

[37] S. Li, M. L. Steigerwald, and L. E. Brus, "Surface states in the photoionization of high-quality CdSe core/shell nanocrystals," *Amer. Chem. Soc. Nano*, vol. 3, no. 5, pp. 1267–1273, May 2009, doi: 10.1021/nn900189f.

[38] A. M. Munro, I. Jen-La Plante, M. S. Ng, and D. S. Ginger, "Quantitative study of the effects of surface ligand concentration on CdSe nanocrystal photoluminescence," *J. Phys. Chem. C*, vol. 111, no. 17, pp. 6220–6227, May 2007, doi: 10.1021/jp068733e.

[39] D. C. J. Neo et al., "Influence of shell thickness and surface passivation on PbS/CdS core/shell colloidal quantum dot solar cells," *Chem. Mater.*, vol. 26, no. 13, pp. 4004–4013, Jul. 2014, doi: 10.1021/cm501595u.

[40] X.-S. Wang, T. E. Dykstra, M. R. Salvador, I. Manners, G. D. Scholes, and M. A. Winnik, "Surface passivation of luminescent colloidal quantum dots with poly (dimethylaminoethyl methacrylate) through a ligand exchange process," *J. Amer. Chem. Soc.*, vol. 126, no. 25, pp. 7784–7785, Jun. 2004, doi: 10.1021/ja0489339.

[41] B. Mahler, N. Lequeux, and B. Dubertret, "Ligand-controlled polytypism of thick-shell CdSe/CdS nanocrystals," *J. Amer. Chem. Soc.*, vol. 132, no. 3, pp. 953–959, Jan. 2010, doi: 10.1021/ja9034973.

[42] A. M. Munro et al., "Colloidal CdSe quantum dot electroluminescence: Ligands and light-emitting diodes," *Microchimica Acta*, vol. 160, no. 3, pp. 345–350, Mar. 2008, doi: 10.1007/s00604-007-0770-7.

[43] R. Wang, Y. Shang, P. Kanjanaboos, W. Zhou, Z. Ning, and E. H. Sargent, "Colloidal quantum dot ligand engineering for high performance solar cells," *Energy Environ. Sci.*, vol. 9, no. 4, pp. 1130–1143, 2016, doi: 10.1039/C5EE03887A.

[44] O. Chen et al., "Compact high-quality CdSe–CdS core–shell nanocrystals with narrow emission linewidths and suppressed blinking," *Nature Mater.*, vol. 12, no. 5, pp. 445–451, May 2013, doi: 10.1038/nmat3539.

[45] H. Shen et al., "Visible quantum dot light-emitting diodes with simultaneous high brightness and efficiency," *Nature Photon.*, vol. 13, no. 3, pp. 192–197, Mar. 2019, doi: 10.1038/s41566-019-0364-z.

[46] L. Wang et al., "Blue quantum dot light-emitting diodes with high electroluminescent efficiency," *Amer. Chem. Soc. Appl. Mater. Interfaces*, vol. 9, no. 44, pp. 38755–38760, Nov. 2017, doi: 10.1021/acsami.7b10785.

[47] "Cadmium selenide quantum dots," Jan. 2022. [Online]. Available: https://www.mesolight.com/CadmiumBasedQuantumDots/19.html

[48] Y. Yang et al., "High-efficiency light-emitting devices based on quantum dots with tailored nanostructures," *Nature Photon.*, vol. 9, no. 4, pp. 259–266, Apr. 2015, doi: 10.1038/nphoton.2015.36.

[49] Y. Sun, Y. Jiang, H. Peng, J. Wei, S. Zhang, and S. Chen, "Efficient quantum dot light-emitting diodes with a $Zn_{0.85}$ $Mg_{0.15}$ O interfacial modification layer," *Nanoscale*, vol. 9, no. 26, pp. 8962–8969, 2017, doi: 10.1039/C7NR02099F.

[50] P. Shen et al., "Solution-processed double-junction quantum-dot light-emitting diodes with an EQE of over 40%," *Amer. Chem. Soc. Appl. Mater. Interfaces*, vol. 11, no. 1, pp. 1065–1070, Jan. 2019, doi: 10.1021/acsami.8b18940.

[51] K. Kim et al., "Zinc oxo clusters improve the optoelectronic properties on indium phosphide quantum dots," *Chem. Mater.*, vol. 32, no. 7, pp. 2795–2802, Apr. 2020, doi: 10.1021/acs.chemmater.9b04309.

[52] K.-H. Kim et al., "Cation-exchange-derived InGaP alloy quantum dots toward blue emissivity," *Chem. Mater.*, vol. 32, no. 8, pp. 3537–3544, Apr. 2020, doi: 10.1021/acs.chemmater.0c00551.

[53] S. Kim et al., "Efficient blue-light-emitting Cd-free colloidal quantum well and its application in electroluminescent devices," *Chem. Mater.*, vol. 32, no. 12, pp. 5200–5207, Jun. 2020, doi: 10.1021/acs.chemmater.0c01275.

[54] T. Kim et al., "Efficient and stable blue quantum dot light-emitting diode," *Nature*, vol. 586, no. 7829, pp. 385–389, Oct. 2020, doi: 10.1038/s41586-020-2791-x.

[55] Y. Sun, Y. Jiang, X. W. Sun, S. Zhang, and S. Chen, "Beyond OLED: Efficient quantum dot light-emitting diodes for display and lighting application," *Chem. Rec.*, vol. 19, no. 8, pp. 1729–1752, Aug. 2019, doi: 10.1002/tcr.201800191.

[56] S. Coe-Sullivan, W.-K. Woo, J. S. Steckel, M. Bawendi, and V. Bulović, "Tuning the performance of hybrid organic/inorganic quantum dot light-emitting devices," *Org. Electron.*, vol. 4, no. 2/3, pp. 123–130, Sep. 2003, doi: 10.1016/j.orgel.2003.08.016.

[57] S. Y. Bang et al., "Highly stable and scalable blue QD-LED via an evaporated TiO_2 thin film as an electron transport layer," *Adv. Opt. Mater.*, vol. 8, no. 21, Nov. 2020, Art. no. 2001172, doi: 10.1002/adom.202001172.

[58] D. Shin et al., "Waterproof flexible InP@ZnSeS quantum dot light-emitting diode," *Adv. Opt. Mater.*, vol. 8, no. 6, Mar. 2020, Art. no. 1901362, doi: 10.1002/adom.201901362.

[59] J. Zhao, J. Zhang, C. Jiang, J. Bohnenberger, T. Basché, and A. Mews, "Electroluminescence from isolated CdSe/ZnS quantum dots in multilayered light-emitting diodes," *J. Appl. Phys.*, vol. 96, no. 6, pp. 3206–3210, Sep. 2004, doi: 10.1063/1.1784611.

[60] W. Ji et al., "High color purity ZnSe/ZnS core/shell quantum dot based blue light emitting diodes with an inverted device structure," *Appl. Phys. Lett.*, vol. 103, no. 5, Jul. 2013, Art. no. 053106, doi: 10.1063/1.4817086.

[61] W. Ji, P. Jing, J. Zhao, X. Liu, A. Wang, and H. Li, "Inverted CdSe/CdS/ZnS quantum dot light emitting devices with titanium dioxide as an electron-injection contact," *Nanoscale*, vol. 5, no. 8, pp. 3474–3480, 2013, doi: 10.1039/c3nr34168b.

[62] J. Lim et al., "Highly efficient cadmium-free quantum dot light-emitting diodes enabled by the direct formation of excitons within InP@ZnSeS quantum dots," *Amer. Chem. Soc. Nano*, vol. 7, no. 10, pp. 9019–9026, Oct. 2013, doi: 10.1021/nn403594j.

[63] C. Jiang et al., "Improved performance of inverted quantum dots light emitting devices by introducing double hole transport layers," *Org. Electron.*, vol. 31, pp. 82–89, Apr. 2016, doi: 10.1016/j.orgel.2016.01.009.

[64] K.-H. Lee et al., "Over 40 cd/A efficient green quantum dot electroluminescent device comprising uniquely large-sized quantum dots," *Amer. Chem. Soc. Nano*, vol. 8, no. 5, pp. 4893–4901, May 2014, doi: 10.1021/nn500852g.

[65] X. Gao and S. S. Yee, "Hole capture cross section and emission coefficient of defect centers related to high-field-induced positive charges in SiO_2 layers," *Solid-State Electron.*, vol. 39, no. 3, pp. 399–403, Mar. 1996, doi: 10.1016/0038-1101(95)00128-X.

[66] U. K. Verma and B. Kumar, "Charge transport in quantum dot organic solar cells with Si quantum dots sandwiched between poly(3-hexylthiophene) (P3HT) absorber and bathocuproine (BCP) transport layers," *J. Appl. Phys.*, vol. 122, no. 15, Oct. 2017, Art. no. 153104, doi: 10.1063/1.4996845.

[67] B. Kumar, S. A. Campbell, and P. P. Ruden, "Modeling charge transport in quantum dot light emitting devices with NiO and ZnO transport layers and Si quantum dots," *J. Appl. Phys.*, vol. 114, no. 4, Jul. 2013, Art. no. 044507, doi: 10.1063/1.4816680.

[68] F. Vahabzad, A. Rostami, M. Dolatyari, G. Rostami, and I. S. Amiri, "Solution-processed QD-LEDs in visible range: Modulation bandwidth enhancement," *Physica B: Condens. Matter*, vol. 574, Dec. 2019, Art. no. 411667, doi: 10.1016/j.physb.2019.411667.

[69] A. Alexandrov, M. Zvaigzne, D. Lypenko, I. Nabiev, and P. Samokhvalov, "Al-, Ga-, Mg-, or Li-doped zinc oxide nanoparticles as electron transport layers for quantum dot light-emitting diodes," *Sci. Rep.*, vol. 10, no. 1, May 2020, Art. no. 7496, doi: 10.1038/s41598-020-64263-2.

[70] X. Dai et al., "Solution-processed, high-performance light-emitting diodes based on quantum dots," *Nature*, vol. 515, no. 7525, pp. 96–99, Nov. 2014, doi: 10.1038/nature13829.

[71] T. Lee, D. Hahm, K. Kim, W. K. Bae, C. Lee, and J. Kwak, "Highly efficient and bright inverted top-emitting InP quantum dot light-emitting diodes introducing a hole-suppressing interlayer," *Small*, vol. 15, no. 50, Dec. 2019, Art. no. 1905162, doi: 10.1002/smll.201905162.

[72] H. Zhang, S. Chen, and X. W. Sun, "Efficient red/green/blue tandem quantum-dot light-emitting diodes with external quantum efficiency exceeding 21%," *Amer. Chem. Soc. Nano*, vol. 12, no. 1, pp. 697–704, Jan. 2018, doi: 10.1021/acsnano.7b07867.

[73] J. Zhao et al., "Efficient CdSe/CdS quantum dot light-emitting diodes using a thermally polymerized hole transport layer," *Nano Lett.*, vol. 6, no. 3, pp. 463–467, Mar. 2006, doi: 10.1021/nl052417e.

[74] A. Rizzo, M. Mazzeo, M. Biasiucci, R. Cingolani, and G. Gigli, "White electroluminescence from a microcontact-printing-deposited CdSe/ZnS colloidal quantum-dot monolayer," *Small*, vol. 4, no. 12, pp. 2143–2147, Dec. 2008, doi: 10.1002/smll.200800350.

[75] P. Yang, L. Zhang, D. J. Kang, R. Strahl, and T. Kraus, "High-resolution inkjet printing of quantum dot light-emitting microdiode arrays," *Adv. Opt. Mater.*, vol. 8, no. 1, Jan. 2020, Art. no. 1901429, doi: 10.1002/adom.201901429.

[76] H. Lee et al., "Air stable eco-friendly quantum dots with a light-mediated photoinitiator for an inkjet printed flexible light emitting diode," *J. Mater. Chem. C*, vol. 10, no. 29, pp. 10708–10718, 2022, doi: 10.1039/D2TC00851C.

[77] S. Zhan et al., "Inkjet-printed multi-color arrays based on eco-friendly quantum dot light emitting diodes with tailored hole transport layer," *J. Soc. Inf. Display*, vol. 30, no. 10, pp. 748–757, Oct. 2022, doi: 10.1002/jsid.1133.

[78] Y. Nakanishi et al., "Active matrix QD-LED with top emission structure by UV lithography for RGB patterning," *J. Soc. Inf. Display*, vol. 28, no. 6, pp. 499–508, Jun. 2020, doi: 10.1002/jsid.910.

[79] J.-S. Park et al., "Alternative patterning process for realization of large-area, full-color, active quantum dot display," *Nano Lett.*, vol. 16, pp. 6946–6953, Oct. 2016, doi: 10.1021/acs.nanolett.6b03007.

[80] W. Mei et al., "High-resolution, full-color quantum dot light-emitting diode display fabricated via photolithography approach," *Nano Res.*, vol. 13, no. 9, pp. 2485–2491, Jun. 2020, doi: 10.1007/s12274-020-2883-9.

[81] K. M. Song et al., "Noninvasive and direct patterning of high-resolution full-color quantum dot arrays by programmed microwetting," *Amer. Chem. Soc. Nano*, vol. 16, no. 10, pp. 16598–16607, Oct. 2022, doi: 10.1021/acsnano.2c06032.

[82] J. Yang et al., "High-resolution patterning of colloidal quantum dots via non-destructive, light-driven ligand crosslinking," *Nature Commun.*, vol. 11, no. 1, Jun. 2020, Art. no. 2874, doi: 10.1038/s41467-020-16652-4.

[83] H. Cho et al., "Direct optical patterning of quantum dot light-emitting diodes via in situ ligand exchange," *Adv. Mater.*, vol. 32, no. 46, Nov. 2020, Art. no. 2003805, doi: 10.1002/adma.202003805.

[84] J. Yang et al., "Nondestructive photopatterning of heavy-metal-free quantum dots," *Adv. Mater.*, vol. 34, no. 43, Oct. 2022, Art. no. 2205504, doi: 10.1002/adma.202205504.

[85] D. Hahm et al., "Direct patterning of colloidal quantum dots with adaptable dual-ligand surface," *Nature Nanotechnol.*, vol. 17, no. 9, pp. 952–958, Sep. 2022, doi: 10.1038/s41565-022-01182-5.

[86] P. Xiao et al., "Surface passivation of intensely luminescent all-inorganic nanocrystals and their direct optical patterning," *Nature Commun.*, vol. 14, no. 1, Jan. 2023, Art. no. 49, doi: 10.1038/s41467-022-35702-7.

[87] A. Carlson, A. M. Bowen, Y. Huang, R. G. Nuzzo, and J. A. Rogers, "Transfer printing techniques for materials assembly and micro/nanodevice fabrication," *Adv. Mater.*, vol. 24, no. 39, pp. 5284–5318, Oct. 2012, doi: 10.1002/adma.201201386.

[88] S. Lee, D. Yoon, D. Choi, and T.-H. Kim, "Mechanical characterizations of high-quality quantum dot arrays via transfer printing," *Nanotechnology*, vol. 24, no. 2, Jan. 2013, Art. no. 025702, doi: 10.1088/0957-4484/24/2/025702.

[89] B. H. Kim et al., "Multilayer transfer printing for pixelated, multicolor quantum dot light-emitting diodes," *Amer. Chem. Soc. Nano*, vol. 10, no. 5, pp. 4920–4925, May 2016, doi: 10.1021/acsnano.5b06387.

[90] S. Coe-Sullivan, J. S. Steckel, W.-K. Woo, M. G. Bawendi, and V. Bulović, "Large-area ordered quantum-dot monolayers via phase separation during spin-casting," *Adv. Funct. Mater.*, vol. 15, no. 7, pp. 1117–1124, Jul. 2005, doi: 10.1002/adfm.200400468.

[91] L. Kim, P. O. Anikeeva, S. A. Coe-Sullivan, J. S. Steckel, M. G. Bawendi, and V. Bulović, "Contact printing of quantum dot light-emitting devices," *Nano Lett.*, vol. 8, no. 12, pp. 4513–4517, Dec. 2008, doi: 10.1021/nl8025218.

[92] T.-H. Kim et al., "Heterogeneous stacking of nanodot monolayers by dry pick-and-place transfer and its applications in quantum dot light-emitting diodes," *Nature Commun.*, vol. 4, no. 1, Nov. 2013, Art. no. 2637, doi: 10.1038/ncomms3637.

[93] M. K. Choi et al., "Wearable red–green–blue quantum dot light-emitting diode array using high-resolution intaglio transfer printing," *Nature Commun.*, vol. 6, no. 1, May 2015, Art. no. 7149, doi: 10.1038/ncomms8149.

[94] S. Y. Kim et al., "Effects of the surface ligands of quantum dots on the intaglio transfer printing process," *Appl. Surf. Sci.*, vol. 610, Feb. 2023, Art. no. 155579, doi: 10.1016/j.apsusc.2022.155579.

[95] T. W. Nam et al., "Thermodynamic-driven polychromatic quantum dot patterning for light-emitting diodes beyond eye-limiting resolution," *Nature Commun.*, vol. 11, no. 1, Jun. 2020, Art. no. 3040, doi: 10.1038/s41467-020-16865-7.

[96] T. Meng et al., "Ultrahigh-resolution quantum-dot light-emitting diodes," *Nature Photon.*, vol. 16, no. 4, pp. 297–303, Apr. 2022, doi: 10.1038/s41566-022-00960-w.

[97] K.-S. Cho et al., "High-performance crosslinked colloidal quantum-dot light-emitting diodes," *Nature Photon.*, vol. 3, pp. 341–345, Jun. 2009, doi: 10.1038/NPHOTON.2009.92.

[98] Y. Li et al., "Developing AMQLED technology for display applications," *SID Symp. Dig. Tech. Papers*, vol. 49, no. 1, pp. 1076–1079, May 2018, doi: 10.1002/sdtp.12130.

[99] Y. Li et al., "Development of high efficiency QLED technology for display applications," *SID Symp. Dig. Tech. Papers*, vol. 53, no. 1, pp. 61–64, Jun. 2022, doi: 10.1002/sdtp.15416.

[100] M. Kanehiro et al., "Challenges for realizing QD-LED display," *SID Symp. Dig. Tech. Papers*, vol. 52, no. 1, pp. 933–936, May 2021, doi: 10.1002/sdtp.14841.

[101] Y. Nakanishi et al., "Development of active-matrix NanoLED display using heavy-metal-free QDs patterned by photolithography process," *SID Symp. Dig. Tech. Papers*, vol. 53, no. 1, pp. 65–68, Jun. 2022, doi: 10.1002/sdtp.15417.

[102] M. Park et al., "All inkjet-printed 6.9500 217 ppi active matrix QD-LED display with RGB Cd-free QDs in the top-emission device structure," *J. Soc. Inf. Display*, vol. 30, no. 5, pp. 433–440, May 2022, doi: 10.1002/jsid.1126.